

# Utilizing 5G NR SSB Blocks for Passive Detection and Localization of Low-Altitude Drones

Palatip Jopanya, Diana P. M. Osorio

Department of Electrical Engineering, Linköping University, Sweden

E-mail: {palatip.jopanya, diana.moya.osorio}@liu.se

**Abstract**—With the exponential growth of the unmanned aerial vehicle (UAV) industry and a broad range of applications expected to appear in the coming years, the employment of traditional radar systems is becoming increasingly cumbersome for UAV supervision. Motivated by this emerging challenge, this paper investigates the feasibility of employing integrated sensing and communication (ISAC) systems implemented over current and future wireless networks to perform this task. We propose a sensing mechanism based on the synchronization signal block (SSB) in the fifth-generation (5G) standard that performs sensing in a passive bistatic setting. By assuming planar arrays at the sensing nodes and according to the 5G standard, we consider that the SSB signal is sent in a grid of orthogonal beams that are multiplexed in time, with some of them pointing toward a surveillance region where low-altitude drones can be flying. The Crámer-Rao Bound (CRB) is derived as the theoretical bound for range and velocity estimation. Our results demonstrate the potential of employing SSB signals for UAV-like target localization at low SNR.

**Index Terms**—Crámer-Rao Bound, integrated sensing and communications, SSB block, UAV intruder detection and localization.

## I. INTRODUCTION

The road toward the standardization of integrated sensing and communication (ISAC) has already started with the 3rd Generation Partnership Project (3GPP) presenting a feasibility study with 32 use cases and potential requirements in Release 19 [1]. Among others, it is expected that fifth-generation (5G) radio signals can be used to sense the presence or proximity of unmanned aerial vehicles (UAVs) illegally flying in restricted areas (e.g. airports, and military bases), which comes as a challenging while critical use case.

In ISAC systems, where the same hardware, waveform, and time-frequency resources are reused for both functionalities, a more efficient use of resources can be achieved, thus avoiding interferences that can appear between communication and radar systems operating simultaneously.

One way to implement ISAC systems is in a passive sensing setting, where communication signals are used as illuminators of opportunity for sensing. Although the abundant downlink data symbols may appear suitable as illuminators of opportunity, they are not ideal candidates for a few reasons.

First, the transmitting beams are focused at random terminal locations by employing i.e., maximum-ratio transmission (MRT) or zero-forcing (ZF) precoders, leaving gaps of weak signal in the surveillance area. Furthermore, the dependency on traffic demands limits their availability.

Pilot signals have shown advantageous passive detection performance. For instance, the work in [2] investigates the positioning reference signal (PRS) for radar sensing. Moreover, the synchronization signal/physical broadcast channel block (SSB) of 5G NR is the only periodic block of symbols that is well-defined as a fixed-size block in the time-frequency grid. SSB is used for cell search when a user equipment (UE) first enters the coverage area of the system, as it is periodically swept across the entire coverage area of the base station [3]. Cell search is carried out continuously by UEs moving between cells, when the UE is in connected or idle mode [3]. Thus, all these characteristics make this block highly appealing for passive sensing in ISAC networks and have been investigated in [4], [5].

Inspired by the promising insights reported in the above works, this paper further proposes a mechanism based on SSB signals for performing passive sensing of UAVs in a surveillance region, which can be also used, for instance, to detect intruders in non-flying zones. We consider a bistatic implementation employing uniform planar arrays (UPAs) at both transmitter and sensing receiver base stations. Our mechanism considers that a number of beams during the SSB procedure are directed toward the surveillance area at higher altitudes, while the rest are directed toward UEs at lower altitudes. The transmit signals are SSB block signals, precoded into a grid of orthogonal beams that sweep across the entire coverage, in a time-multiplexed fashion. For this system, we derive the Crámer-Rao bound (CRB) for range and velocity estimation and compare it with the two-dimensional fast Fourier transform (2D-FFT) estimation method. For the 2D-FFT, we consider a receiver beam aggregation criterion based on a peak-to-average factor (PAF) of the range-velocity profile for the estimation. Additionally, we provide insights on the impact of system parameters and evaluate the impact of the number of beams directed toward the surveillance region over the detection performance.

## II. SYSTEM MODEL

We consider a pair of multiple-input multiple-output (MIMO) ISAC base stations (BSs) that jointly form a bistatic sensing pair consisting of base station A (BsA), which functions as the sensing transmitter, and base station B (BsB), which functions as the sensing receiver, while both BSs are capable of transmitting and receiving communication symbols. We assume that BsA and BsB are coordinated and synchro-

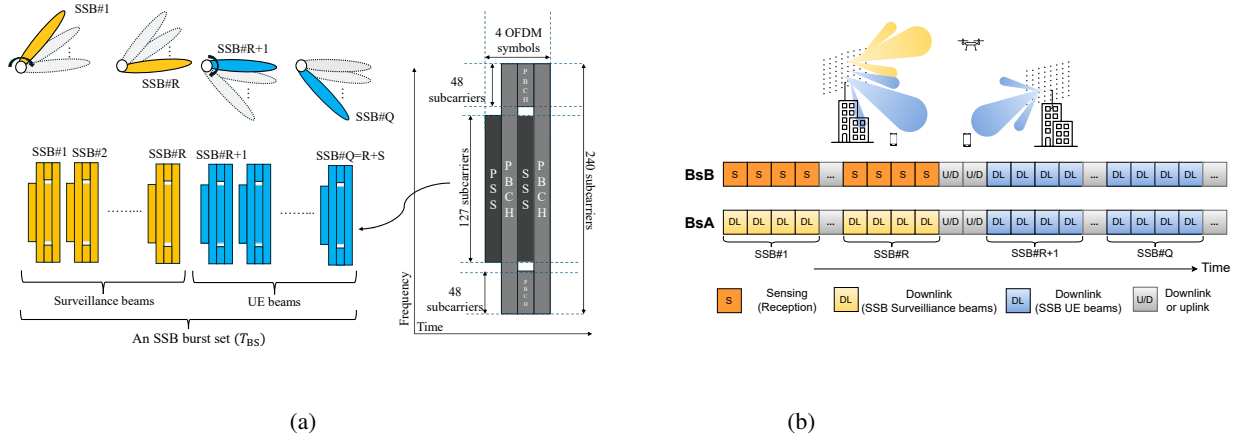


Fig. 1: a) An SSB scheduling, b) Dynamic TDD flow with sensing reception.

nized in phase and frequency. BsA and BsB are equipped with a UPA with  $M_H$  antennas per row and  $M_V$  antennas per column with  $M_V=M_H$  that add up to  $M=M_V \times M_H$  total antennas. The system operates in dynamic time-division duplexing (TDD) workflow, wherein BsB switches to reception mode when BsA transmits sensing symbols as illustrated in Fig. 1b. The BSs serve user equipments (UEs) via data symbols and synchronize with UEs via SSB symbols. We propose that the BsB exploits the echoes from the beam sweeping of the SSB beams directed toward the surveillance area, referred to as surveillance beams. The illustration of the bistatic setup in upper part of Fig. 1b shows the beam sweep of surveillance beams in yellow and the SSBs of UEs in blue.

#### A. Synchronization Signal Block (SSB)

In the 5G standard, an SSB is a periodic signal that is structured as a block of orthogonal frequency-division multiplexing (OFDM) symbols consisting of PSS (Primary Synchronization Signal), SSS (Secondary Synchronization Signal), and Physical Broadcast Channel (PBCH) symbols, as shown in Fig. 1a. Each block is transmitted consecutively in time with a few symbols as a gap in different directions and time. A set of SSB blocks, called an SSB burst set, covers the entire surveillance area and UEs coverage. This sweeping process is confined within  $T_{BS}$  (SSB burst set period) and will be repeated periodically in every SSB periodicity, as shown in Fig. 1a [3].

#### B. Transmit signal

An OFDM block with  $N$  subcarriers and  $L$  symbols is considered. The baseband signal of the  $n$ th subcarrier and  $l$ th symbol can be written as [6]  $x_{n,l}(t) = \sqrt{\rho} x_{n,l} e^{j2\pi n f_{\Delta} t} \text{rect}\left(\frac{t-T_s}{T_s}\right)$ , where  $n = [1, 2, \dots, N]$  is the subcarrier index,  $l = [1, 2, \dots, L]$  is the symbol index,  $x_{n,l}$  is the complex data corresponding to the  $n$ th subcarrier and  $l$ th symbol,  $\rho$  is the transmitted power per symbol,  $f_{\Delta}$  is subcarrier spacing,  $T_s = \frac{1}{f_{\Delta}}$  is symbol duration,  $T = T_s + T_c$  is the total symbol duration, and  $T_c$  is the cyclic

prefix duration. We assume that the cyclic prefix is larger than the delay spread of the targets. The antenna steering vector of  $r$ th beam,  $\mathbf{a}(\theta_r, \phi_r) \in \mathbb{C}^M$ , is a half-wavelength spaced UPA antenna response, where  $\theta_r$  is the azimuth and  $\phi_r$  is the elevation of  $r$ th beam. This is defined as [7]  $\mathbf{a}(\theta_r, \phi_r) = \mathbf{a}_{M_V}(\phi_r, 0) \otimes \mathbf{a}_{M_H}(\theta_r, \phi_r)$ , with  $\mathbf{a}_{M_V}(\phi_r, 0) = [1, e^{-j\pi \sin(\phi_r)}, \dots, e^{-j\pi(M_V-1) \sin(\phi_r)}]^T$ ,  $\mathbf{a}_{M_H}(\theta_r, \phi_r) = [1, e^{-j\pi \sin(\theta_r) \cos(\phi_r)}, \dots, e^{-j\pi(M_H-1) \sin(\theta_r) \cos(\phi_r)}]^T$ , where  $\mathbf{a}_{M_H}(\theta_r, \phi_r) \in \mathbb{C}^{M_H}$  and  $\mathbf{a}_{M_V}(\phi_r, 0) \in \mathbb{C}^{M_V}$ . We design a grid of beams that provides a set of angles in the antenna response as

$$\{\mathbf{a}(\theta_i, \phi_j)\}; \theta_i = \arcsin\left(\frac{2q}{\sqrt{M}}\right), \phi_j = \arcsin\left(\frac{2q}{\sqrt{M}}\right), \quad (1)$$

for  $q \in \{0, \pm 1, \pm 2, \dots, \lfloor \frac{\sqrt{M}}{2} - 1 \rfloor\}$ , where each antenna response corresponds to each beam. For instance,  $M=100$  results in 9 angles in degrees as  $\theta_i, \phi_j \in \{0, \pm 11.5, \pm 23.6, \pm 36.9, \pm 53.1\}$ , yielding a total of 81 antenna responses in a set. Define the normalized precoder matrix  $\mathbf{F} \in \mathbb{C}^{M \times R}$  as

$$\mathbf{F} = \frac{1}{\sqrt{M}} [\mathbf{a}^*(\theta_1, \phi_1), \mathbf{a}^*(\theta_2, \phi_2), \dots, \mathbf{a}^*(\theta_R, \phi_R)], \quad (2)$$

where each column represents a unique, conjugate-normalized antenna response in a given set in (1). Note that we consider only a total of  $R$  beams in the surveillance area, with an elevation greater than zero. The passband transmitted signal can be written as  $\text{Re}\{x_{n,l,r} \mathbf{f}_r e^{j2\pi f_c t}\}$ , where  $f_c$  is the carrier frequency,  $\mathbf{f}_r$  is the  $r$ th column in matrix  $\mathbf{F}$  in (2), and  $x_{n,l,r}$  is symbol  $x_{n,l}$  of SSB beam  $r$ th. Define  $\Phi \in \mathbb{C}^{R \times R}$ , a diagonal matrix with sequence of unit power symbols in the diagonal,  $\Phi \Phi^H = \mathbf{I}_R$ . This yields,  $\text{Re}\{\mathbf{F} \Phi e^{j2\pi f_c t}\}$ , a sequence of transmitting symbols in grid of orthogonal beams.

#### C. Received signal

We consider only the echoes from surveillance beams, where the clutter is assumed to be stationary. Furthermore, the clutter from non-target objects in both line-of-sight (LoS) and

non-line-of-sight (NLoS) conditions is assumed to be removed by the system. A study in [8] demonstrates an OFDM-based clutter rejection method. The channel consists of the LoS direct-link between BsA and BsB and the echoes from the targets. The received signal,  $\mathbf{y}_{n,l,r} \in \mathbb{C}^M$ , of  $n$ th subcarrier,  $l$ th symbol, and  $r$ th beam with a delay shift  $\tau$  and a Doppler effect  $f_d$  in discrete time is given by [9], [6]

$$\mathbf{y}_{n,l,r} = \sqrt{\rho} x_{n,l,r}(lT_s - \tau) \mathbf{H} \mathbf{f}_r e^{j2\pi f_d l T_s} + \mathbf{w}_{n,l}, \quad (3)$$

where  $\mathbf{H} \in \mathbb{C}^{M \times M}$  is the channel, and  $\mathbf{w}_{n,l} \sim \mathcal{CN}(0, \sigma_n^2 \mathbf{I})$  is additive white Gaussian noise (AWGN). The transmit symbols are removed at the BsB assuming that they are known by coordination. Thus,  $\mathbf{Y}_{n,l} \Phi^H = \sqrt{\rho} \mathbf{H} \mathbf{F} \Phi \Phi^H + \mathbf{W}' = \sqrt{\rho} \mathbf{H} \mathbf{F} + \mathbf{W}'$ , where  $\mathbf{Y}_{n,l} \in \mathbb{C}^{M \times R}$  is a matrix of the received sequence, and  $\mathbf{W}' = \mathbf{W} \Phi^H$ . The received signal,  $\mathbf{Y}'_{n,l} = \mathbf{Y}_{n,l} \Phi^H$ ,  $\mathbf{Y}'_{n,l} \in \mathbb{C}^{M \times R}$ , can be derived to account for the direct link and the echoes as follows:

$$\begin{aligned} \mathbf{Y}'_{n,l} = & \underbrace{\sqrt{\rho} \beta_0 \mathbf{H}_0 \mathbf{F} e^{-j2\pi(f_c + n f_\Delta) \tau_0}}_{\text{Direct link}} \\ & + \underbrace{\sqrt{\rho} \sum_{k=1}^K \alpha_k \sqrt{\beta_k} \mathbf{a}(\theta_{a,k}, \phi_{a,k}) \mathbf{a}^T(\theta_{d,k}, \phi_{d,k}) \mathbf{F}}_{\substack{\text{Arrival} \quad \text{Departure} \\ \text{echoes}}} \\ & \underbrace{e^{-j2\pi(f_c + n f_\Delta) \tau_k} e^{j2\pi f_{d,k} l T_s}}_{\substack{\text{Delay shift} \quad \text{Doppler effect}}} + \mathbf{W}'_{n,l}, \end{aligned} \quad (4)$$

where  $K$  is the number of targets,  $\beta_0$  is the channel gain from direct link,  $\mathbf{H}_0$  is the direct link channel,  $\theta_{a,k}, \phi_{a,k}$  are arrival azimuth and arrival elevation of  $k$ th target, respectively, corresponding to BsB,  $\theta_{d,k}, \phi_{d,k}$  are departure azimuth and departure elevation of  $k$ th target, respectively, corresponding to BsA,  $\tau_k$  is the total delay of the echoes of target  $k$ th,  $f_{d,k}$  is the Doppler shift effect from target  $k$ th, and  $\alpha_k \sim \mathcal{CN}(0, 1)$  is the randomness model of a radar cross section (RCS) of the  $k$ th target that follows a Swerling 1 model, where the realization fluctuates slowly and remains fixed within the OFDM block length  $L$ .  $\beta_k$  is the channel gain of the echoes, BsA-target  $k$ th-BsB, that is

$$\beta_k = \frac{\lambda_c^2 \sigma_{\text{RCS},k}}{(4\pi)^3 d_{\text{Tx},k}^2 d_{\text{k},r,x}^2}, \quad (5)$$

where  $\lambda_c$  is a wavelength of the carrier frequency,  $d_{\text{Tx},k}$  is the distance between BsA and target  $k$ th,  $d_{\text{k},r,x}$  is the distance between target  $k$ th and BsB, and  $\sigma_{\text{RCS}}$  is the RCS in dBsm. We assume that the first term (direct link) in (4) is known and can be removed at BsB since both BsA and BsB are stationary. The received signal,  $\mathbf{Y}'_{n,l}$ , after direct link cancellation, down-conversion and substituting the Doppler shift with velocity ( $f_{d,k} = \frac{2v_k}{\lambda_c}$ ) and the delay with the bistatic range ( $\tau = \frac{d_k}{c}$ ) is

$$\begin{aligned} \mathbf{Y}'_{n,l} = & \sqrt{\rho} \sum_{k=1}^K \alpha_k \sqrt{\beta_k} \mathbf{a}(\theta_{a,k}, \phi_{a,k}) \mathbf{a}^T(\theta_{d,k}, \phi_{d,k}) \mathbf{F} \\ & e^{-j2\pi n f_\Delta \frac{d_k}{c}} e^{j4\pi \frac{v_k}{\lambda_c} l T_s} + \mathbf{W}'_{n,l}, \end{aligned} \quad (6)$$

where  $c$  is the speed of light,  $d_k$  is the bistatic range of target  $k$ th,  $v_k$  is the relative radial velocity of target  $k$ th with respect to the BsB. The unambiguous range is a detectable distance given by the propagated distance of one symbol duration as  $d_u \leq cT_s$ . The unambiguous velocity is the range of maximum and minimum relative radial velocities, which can be defined as  $|v_u| \leq \frac{\lambda_c f_\Delta}{2}$ .

### III. PARAMETERS ESTIMATION

#### A. 2D-FFT

The two-dimensional fast Fourier transform (2D-FFT) is a non-parametric method in spectral estimation [10]. We use 2D-FFT for estimating the range and velocity and to compare it with the CRB. This method is used because 2D-FFT is simple and does not require the number of targets a priori. To implement 2D-FFT in this system, we first form a received frame matrix,  $\mathbf{Z}_r \in \mathbb{C}^{N \times L}$ , of SSB beam  $r$ th disregarding the dimension of  $M$ , multiple antennas. Given that the received signal vector  $\mathbf{y}'_{n,l,r} = [y_{n,l,r,1}, y_{n,l,r,2}, \dots, y_{n,l,r,M}]^T$  is the  $r$ th column of  $\mathbf{Y}'_{n,l}$  in (6).  $\mathbf{Z}_r$  is formed by arranging the first element of each  $\mathbf{y}'_{n,l,r}$  as

$$\mathbf{Z}_r = \begin{bmatrix} y_{1,1,r,1} & y_{1,2,r,1} & \dots & y_{1,L,r,1} \\ y_{2,1,r,1} & y_{2,2,r,1} & \dots & y_{2,L,r,1} \\ \vdots & \vdots & \ddots & \vdots \\ y_{N,1,r,1} & y_{N,2,r,1} & \dots & y_{N,L,r,1} \end{bmatrix}. \quad (7)$$

Define a range-velocity profile as  $\mathbf{Z}'_r \in \mathbb{R}^{N' \times L'}$ , the  $n'$ th row and  $l'$ th column in matrix  $\mathbf{Z}'_r$  is

$$[\mathbf{Z}'_r]_{n',l'} = \left| \sum_{n=0}^{N'-1} \left( \sum_{l=0}^{L'-1} [\mathbf{Z}_r]_{n,l} e^{-j2\pi l' \frac{l}{L'}} \right) e^{j2\pi n' \frac{n}{N'}} \right|, \quad (8)$$

where  $[\mathbf{Z}_r]_{n,l}$  is the  $n$ th row and  $l$ th column in matrix  $\mathbf{Z}_r$ . The range-velocity profile in (8) can be seen as row-wise  $L'$ -point FFT and column-wise  $N'$ -point IFFT of  $\mathbf{Z}_r$  with padding zeros,  $L' > L$ ,  $N' > N$ .

#### B. Received beam aggregation

Since BsB receives a total of  $R$  OFDM blocks with only a few containing target echoes, we propose a received beam aggregation method based on PAF. The PAF of the received beam  $r$ th is defined as  $p_r = \frac{\max_{n',l'} \mathbf{Z}'_r}{1^T \mathbf{Z}'_r \mathbf{1}}$  and the PAF vector is  $\text{PAF} = [p_1, p_2, \dots, p_R]^T$ . Define a set  $\eta$  that satisfies  $\eta = \{i\}$ ,  $i$  s.t.  $p_i > \gamma_a$ ,  $i \in \{1, 2, \dots, R\}$ , where  $\gamma_a$  is a selected threshold. A larger PAF enhances the separation between the target and noise. Define  $\mathbf{Z}'$ , the aggregated profile, as  $\mathbf{Z}' = \frac{1}{|\eta|} \sum_{j \in \eta} \mathbf{Z}'_j$ , where  $|\eta|$  is the size of the set  $\eta$ . For a single target, the bistatic range estimate ( $\hat{d}$ ) and relative velocity estimate ( $\hat{v}$ ) can be found as  $\hat{d} = \frac{\hat{n} c T_s}{N'}$ ,  $\hat{v} = \frac{\hat{l} f_\Delta \lambda_c}{2L'}$ , where  $\hat{n}$  and  $\hat{l}$  are the row and column indices that locate the peak in  $\mathbf{Z}'$  as  $(\hat{n}, \hat{l}) = \text{argmax}_{n',l'} \mathbf{Z}'$ .

### C. Target detection

The detection decision is based on threshold,  $\gamma$ . The detector is given as  $p \stackrel{\mathcal{H}_1}{\geq} \gamma$ , where, the detector indicates the presence of a target when  $p > \gamma$  and the absence of a target if  $p < \gamma$ . Here,  $p$  is defined as  $p = \max_r \text{PAF}$ .

### IV. CRAMÉR-RAO BOUND

For simplicity, we consider the CRB of the random variables, range and velocity, denoted as  $\Theta = [\Theta_i, \Theta_j]^T = [d, v]^T$ , in a single target case ( $K=1$ ). We evaluate this for a given signal-to-noise ratio at BsB,  $\text{SNR}_r = \frac{\rho \beta g^2}{\sigma_n^2 M}$ , assuming a given RCS and fixed flight path. The received signal at the  $n$ th row,  $l$ th column of (7), disregarding the subscript  $r, 1$  and  $k$ , can be rewritten as

$$y_{n,l} = \sqrt{\frac{\rho}{M}} \beta \alpha g e^{-j2\pi n f_{\Delta} \frac{d}{c}} e^{j4\pi \frac{v}{\lambda_c} l T_s} + w_{n,l}, \quad y_{n,l} \in \mathbb{C}, \quad (9)$$

where  $g = \mathbf{a}^T(\theta_d, \phi_d) \mathbf{a}^*(\theta_r, \phi_r)$  is the beamforming gain of the  $r$ th transmitting beam with respect to the target's angle and is bounded by  $M(\text{dB}) - 3.7\text{dB} < |g| \leq M(\text{dB})$  irrespective of whether the target is located inside the grid of orthogonal beams, given that the  $r$ th beam is directed closest to the target among all  $R$  beams. Formulate a vector  $\mathbf{y} = [y_{1,1}, y_{2,1}, \dots, y_{2,1}, y_{2,2}, \dots, y_{N,L}]^T$ ,  $\mathbf{y} \in \mathbb{C}^{NL}$ , from (9), i.e., by flattening  $\mathbf{Y}$ , where  $[\mathbf{Y}]_{n,l} = y_{n,l}$ . The Fisher information,  $\text{FIM}(\Theta)$ , for a complex Gaussian signal, as given in [11, Eq. (15.52)], is defined as

$$[\text{FIM}(\Theta)]_{i,j} = 2\text{Re} \left\{ \frac{\partial \mu_{\mathbf{y}}^H(\Theta)}{\partial \Theta_i} \mathbf{C}_{\mathbf{y}}^{-1}(\Theta) \frac{\partial \mu_{\mathbf{y}}(\Theta)}{\partial \Theta_j} \right\}, \quad (10)$$

where the first term in [11, Eq. (15.52)] is zero,  $\mathbf{C}_{\mathbf{y}} = \sigma_n^2 \mathbf{I}$  is the covariance matrix of  $\mathbf{y}$ , since  $\alpha$  remains constant within an OFDM block length  $L$  in the Swerling 1 model, and  $\mu_{\mathbf{y}} = \sqrt{\frac{\rho}{M}} \beta \alpha g [e^{-j2\pi f_{\Delta} \frac{d}{c}} e^{j4\pi \frac{v}{\lambda_c} T_s}, \dots, e^{-j2\pi N f_{\Delta} \frac{d}{c}} e^{j4\pi \frac{v}{\lambda_c} L T_s}]^T$  is the mean of  $\mathbf{y}$ .

**Proposition 1.** *The lower bound on the variance of the distance estimates is*

$$\text{var}\{\hat{d}\} \geq \frac{3T_s^2 c^2 (2L+1)}{\pi^2 \text{SNR}_r N L (7NL - N - L - 5)(N+1)}, \quad (11)$$

and the bound on the variance of the velocity estimates is

$$\text{var}\{\hat{v}\} \geq \frac{3\lambda_c^2 f_{\Delta}^2 (2N+1)}{4\pi^2 \text{SNR}_r N L (7NL - N - L - 5)(L+1)}, \quad (12)$$

where  $\text{SNR}_r$  is the SNR at BsB after attenuation from pathloss and  $\sigma_{\text{RCS}}$ .

*Proof.* See appendix A.  $\square$

### V. SIMULATION RESULTS

The parameters and values are provided in Table I. Fig. 2 shows the CRB for different configurations of  $N$  and  $L$ . A larger  $N$  lowers the CRB bound for both range and velocity, with a more significant impact on range. Similarly, a larger  $L$  lowers the CRB for both range and velocity, with a greater

TABLE I: Simulation parameters.

Parameter	Value	Parameter	Value
$M_V = M_H$	10	$\sigma_{\text{RCS}}$	-10 dBsm
$f_{\Delta}$	60 kHz	$\gamma_a$	6
$f_c$	15 GHz	R	45

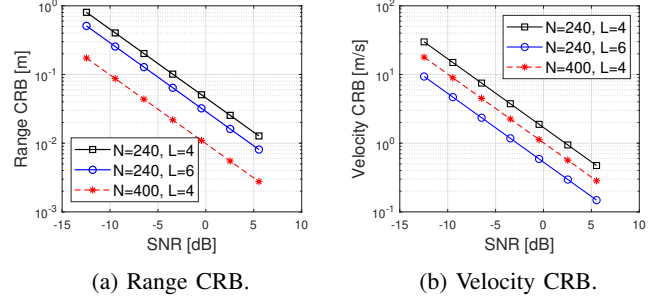


Fig. 2: Range and velocity CRB in different block sizes.

impact on velocity. In Fig. 3, a target is generated with a random range,  $d \leq d_u$ , and random velocity,  $|v| \leq v_u$ . Fig. 3a shows CRB and range root mean square error (RMSE) of an  $N'$ -point IFFT at  $\text{SNR}_r = -10$  dB, where the SSB line represents the received signal nullified at some symbols in the block, as shown in Fig. 1a. Similarly, Fig. 3b shows the CRB and velocity RMSE of  $L'$ -point FFT at  $\text{SNR}_r = -7$  dB. The results show that RMSE values for  $N=240, L=4$ , and the SSB block are approximately the same for both cases, range and velocity. The absence of some symbols in the SSB block has minimal effect compared to the completed block.

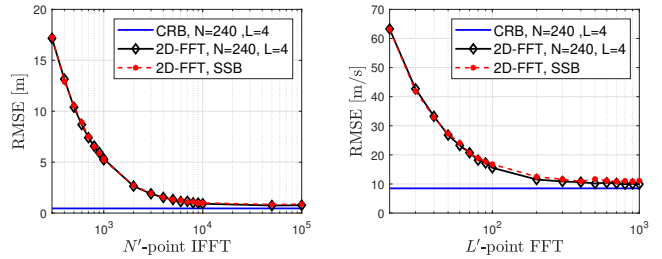


Fig. 3: Range and velocity RMSE at  $\text{SNR}_r = -10$  dB. (a)  $N'$ -point IFFT range RMSE (b)  $L'$ -point FFT velocity RMSE at  $\text{SNR}_r = -7$  dB.

Fig. 3: Range and velocity RMSE.

Furthermore, the detection performance is investigated. The accuracy,  $P_c$ , is defined as  $P_c = \frac{TP+TN}{T_a}$ , where  $TP$  is the number of true positives,  $TN$  is the number of true negatives, and  $T_a$  is the total number of experiments. We also incorporate a power-saving scheme by randomly deactivating a percentage of surveillance beams uniformly. A 100% beam deactivation indicates that all surveillance beams are turned off, while a 0% deactivation means all beams remain active. Fig. 4 shows that with appropriate thresholds,  $\gamma=4$  and  $\gamma=6$ ,  $P_c$  is maintained for up to 20% beam deactivation. Note that the probabilities of the presence and absence of a target are both 0.5.

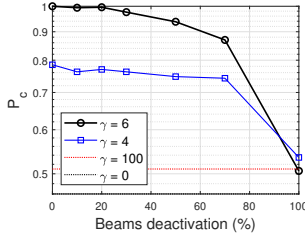


Fig. 4:  $P_c$  of beam deactivation at different  $\gamma$ .

## VI. CONCLUSIONS

This paper investigates target sensing using the SSB with a grid of orthogonal beams. Detection and localization are based on the 2D-FFT, assisted by PAF. The SSB symbols corresponding to the surveillance beams are used as an illuminator in a bistatic setup, with the base station as the sensing node. The simulation results for the given scenario show potential for UAV-like target sensing.

### APPENDIX A PROOF OF PROPOSITION 1

The Fisher information for each element is

$$\begin{aligned} [\text{FIM}(\Theta)]_{d,d} &= 2\text{Re}\left\{4\pi^2 \frac{\rho\beta g^2}{M\sigma_n^2} \mathbb{E}\{|\alpha|^2\} \frac{f_\Delta^2}{c^2} L \sum_{n=1}^N n^2\right\} \\ &= \frac{4}{3}\pi^2 \text{SNR}_r \frac{f_\Delta^2}{c^2} LN(N+1)(2N+1), \end{aligned} \quad (13)$$

$$\begin{aligned} [\text{FIM}(\Theta)]_{v,v} &= 2\text{Re}\left\{16\pi^2 \frac{\rho\beta g^2}{M\sigma_n^2} \mathbb{E}\{|\alpha|^2\} \frac{T_s^2}{\lambda_c^2} N \sum_{l=1}^L l^2\right\} \\ &= \frac{16}{3}\pi^2 \text{SNR}_r \frac{T_s^2}{\lambda_c^2} NL(L+1)(2L+1), \end{aligned} \quad (14)$$

$$\begin{aligned} [\text{FIM}(\Theta)]_{d,v} &= 2\text{Re}\left\{-8\pi^2 \frac{\rho\beta g^2}{M\sigma_n^2} \mathbb{E}\{|\alpha|^2\} \frac{f_\Delta T_s}{c\lambda_c} \sum_{n=1}^N \sum_{l=1}^L nl\right\} \\ &= -4\pi^2 \text{SNR}_r \frac{1}{c\lambda_c} NL(L+1)(N+1), \end{aligned} \quad (15)$$

where  $[\text{FIM}(\Theta)]_{v,d}=[\text{FIM}(\Theta)]_{v,v}$ ,  $\mathbb{E}\{|\alpha|^2\}=1$ ,  $\text{SNR}_r=\frac{\rho\beta g^2}{\sigma_n^2 M}$ ,  $\sum_{n=1}^N n=\frac{N(N+1)}{2}$ ,  $\sum_{n=1}^N n^2=\frac{N(N+1)(2N+1)}{6}$  and  $T_s f_\Delta=1$ . The Fisher information matrix is

$$[\text{FIM}(\Theta)] = 4\pi^2 \text{SNR}_r NL \begin{bmatrix} \frac{1}{3} \frac{f_\Delta^2}{c^2} (N+1)(2N+1) & -\frac{1}{c\lambda_c} (L+1)(N+1) \\ -\frac{1}{c\lambda_c} (L+1)(N+1) & \frac{4}{3} \frac{T_s^2}{\lambda_c^2} (L+1)(2L+1) \end{bmatrix}. \quad (16)$$

Finally, the CRB( $\Theta$ ) can be derived as

$$\begin{aligned} \text{CRB}(\Theta) &= \text{FIM}^{-1}(\Theta) = \frac{1}{4\pi^2 \text{SNR}_r NL \det(\text{FIM}(\Theta))} \\ &= \frac{1}{\pi^2 \text{SNR}_r NL (7NL - N - L - 5)} \\ &\quad \begin{bmatrix} \frac{4}{3} \frac{T_s^2}{\lambda_c^2} (L+1)(2L+1) & \frac{1}{c\lambda_c} (L+1)(N+1) \\ \frac{1}{c\lambda_c} (L+1)(N+1) & \frac{1}{3} \frac{1}{c^2} f_\Delta^2 (N+1)(2N+1) \end{bmatrix} \\ &= \frac{1}{\pi^2 \text{SNR}_r NL (7NL - N - L - 5)} \\ &\quad \begin{bmatrix} 3T_s^2 c^2 \frac{(2L+1)}{(N+1)} & \frac{9}{4} \lambda_c c \\ \frac{9}{4} \lambda_c c & \frac{3}{4} \lambda_c^2 f_\Delta^2 \frac{(2N+1)}{(L+1)} \end{bmatrix}. \end{aligned} \quad (17)$$

### ACKNOWLEDGMENT

This work was supported in part by ELLIIT and in part by WASP-funded project ‘‘ALERT’’.

### REFERENCES

- [1] 3GPP, ‘‘3rd generation partnership project; technical specification group tsg sa; feasibility study on integrated sensing and communication (release 19),’’ 3GPP, Tech. Rep. TR 22.837 V19.4.0 (2024-06), 2024.
- [2] Z. Wei, Y. Wang, L. Ma, S. Yang, Z. Feng, C. Pan, Q. Zhang, Y. Wang, H. Wu, and P. Zhang, ‘‘5G PRS-based sensing: A sensing reference signal approach for joint sensing and communication system,’’ *IEEE Transactions on Vehicular Technology*, vol. 72, no. 3, pp. 3250–3263, 2023.
- [3] J. S. Erik Dahlman, Stefan Parkvall, *5G NR: The Next Generation Wireless Access Technology*. Elsevier Science, 2018.
- [4] K. Abratkiewicz, A. Księżyk, M. Płotka, P. Samczyński, J. Wszolek, and T. P. Zieliński, ‘‘SSB-based signal processing for passive radar using a 5G network,’’ *IEEE Journal of Selected Topics in Applied Earth Observations and Remote Sensing*, vol. 16, pp. 3469–3484, 2023.
- [5] M. Golzadeh, E. Tirola, L. Anttila, J. Talvitie, K. Hooli, O. Tervo, I. Peruga, S. Hakola, and M. Valkama, ‘‘Downlink sensing in 5G-advanced and 6G:SIB1-assisted SSB approach,’’ in *2023 IEEE 97th Vehicular Technology Conference (VTC2023-Spring)*, 2023, pp. 1–7.
- [6] V. Koivunen, M. F. Keskin, H. Wymeersch, M. Valkama, and N. Prelicic, ‘‘Multicarrier ISAC: Advances in waveform design, signal processing, and learning under nonidealities [special issue on signal processing for the integrated sensing and communications revolution],’’ *IEEE Signal Processing Magazine*, vol. 41, pp. 17–30, 09 2024.
- [7] E. Björnson and Ö. Demir, *Introduction to Multiple Antenna Communications and Reconfigurable Surfaces*, ser. NowOpen Series. Now Publishers, 2024. [Online]. Available: <https://books.google.se/books?id=TCZx0AEACAAJ>
- [8] X. Zhou, S. Ding, and X. Li, ‘‘A fast-processing approach for passive ofdm radar clutter rejection,’’ in *2024 14th International Symposium on Antennas, Propagation and EM Theory (ISAP)*, 2024, pp. 1–4.
- [9] D. H. N. Nguyen and R. W. Heath, ‘‘Delay and doppler processing for multi-target detection with IEEE 802.11 OFDM signaling,’’ in *2017 IEEE International Conference on Acoustics, Speech and Signal Processing (ICASSP)*, 2017, pp. 3414–3418.
- [10] C. Sturm and W. Wiesbeck, ‘‘Waveform design and signal processing aspects for fusion of wireless communications and radar sensing,’’ *Proceedings of the IEEE*, vol. 99, no. 7, pp. 1236–1259, 2011.
- [11] S. M. Kay, *Fundamentals of statistical signal processing: estimation theory*. USA: Prentice-Hall, Inc., 1993.